Revista Eletrônica
Acervo Saúde
Electronic Journal Collection Health ISSN 2178-2091

Antitumor and toxicological evaluation of 2-N-glycine-1,4-naphthoquinone in Ehrlich tumor-bearing Swiss mice

Avaliação antitumoral e toxicológica de 2-N-glicina-1,4-naftoquinona no tumor de Ehrlich em camundongos Swiss

Evaluación antitumoral y toxicológica de 2-N-glicina-1,4-naftoquinona en tumor de Ehrlich en ratones Swiss

Elayne Cristine Soares da Silva[1], Fernanda Carolina Ribeiro Dias[2], Celso de Amorim Câmara[3], Sandra Maria de Torres[4], Márcia de Figueiredo Pereira[4], Danielle Barbosa Morais[5], Valdemiro Amaro da Silva Junior[4].

ABSTRACT

Objective: To determine the toxicity of the synthetic derivative 2-N-glycine-1, structurally related to 4-naphthoquinone lapachol, in Swiss male mice following oral administration of this compound. **Methods:** Ehrlich tumors were implanted into the subcutaneous tissue of the right axillary region of 8-week-old Swiss male mice, and the tumor cells were maintained in ascitic form. Treatments began on the third day after tumor cell implantation, and biometric assessments were performed daily until the eighth day. Microsteatosis and hepatic coagulative necrosis, Bowman's capsule thickening, and renal tubular necrosis were most severe with 1000 or 4000 µg/kg. **Results:** Overall, the most effective rate of tumor inhibition was observed in animals treated with 40 µg/kg of the compound, with a percentage reduction ranging from 90% to 96% compared to controls. Naphthoquinone did not exhibit a dose-dependent anticancer effect. However, significant dose-dependent histopathological alterations were observed, particularly in the liver, kidneys, heart, and spleen, as well as a decrease in hematocrit. **Conclusion:** The data demonstrate that while naphthoquinone promoted significant tumor reduction at a dose of 40 µg/kg, this was accompanied by marked dose-dependent toxicity in the liver, kidneys, and heart.

Keywords: Cancer, Ehrlich carcinoma, Histopathology, Medicinal chemistry, Toxicity.

[1] Department of Animal Morphology and Physiology, Federal Rural University of Pernambuco, Recife - PE.
[2] Department of Natural Sciences, Federal University of São João del Rei, São João del Rei - MG.
[3] Department of Chemistry, Federal Rural University of Pernambuco, Recife - PE.
[4] Department of Veterinary Medicine, Federal Rural University of Pernambuco, Recife - PE.
[5] Department of Morphology, Federal University of Rio Grande do Norte, Natal - RN.

SUBMITTED: 3/2026 | **ACCEPTED: 4/2026** | **PUBLISHED: 5/2026**

RESUMO

Objetivo: Determinar a toxicidade do derivado sintético 2-N-glicina-1, estruturalmente relacionado à 4-naftoquinona lapachol, em camundongos machos Swiss após administração oral deste composto. **Métodos:** O tumor de Ehrlich foi implantado no tecido subcutâneo da região axilar direita em camundongos machos Swiss de 8 semanas de idade, e a célula tumoral foi mantida sob forma ascítica. Os tratamentos começaram no 3º dia após a implantação da célula tumoral e a avaliação biométrica foi realizada diariamente até o 8º dia. Microesteatose e necrose da coagulação hepática, espessamento da cápsula de Bowman e necrose do túbulo renal foram mais graves com 1000 ou 4000 µg/kg. **Resultados:** Em geral, a taxa mais efetiva de inibição do tumor foi observada em animais tratados com 40 µg/kg do composto, com uma redução de % variando de 90 a 96% em comparação aos controles. A naftoquinona não exibiu um efeito anticancerígeno dependente da dose. No entanto, alterações histopatológicas significativas foram encontradas de forma dose-dependente, especialmente no fígado, rins, coração e baço, bem como diminuição do hematócrito. **Conclusão:** Os dados demonstram que, embora a naftoquinona tenha promovido redução tumoral significativa na dose de 40 µg/kg, isso foi acompanhado por toxicidade dose-dependente acentuada no fígado, rins e coração.

Palavras-chave: Câncer, Carcinoma de Ehrlich, Histopatologia, Química medicinal, Toxicidade.

RESUMEN

Objetivo: Determinar la toxicidad del derivado sintético 2-N-glicina-1, estructuralmente relacionado con la 4-naftoquinona lapachol, en ratones macho Swiss tras la administración oral de este compuesto. **Métodos:** Se implantaron tumores de Ehrlich en el tejido subcutáneo de la región axilar derecha de ratones macho Swiss de 8 semanas de edad, y las células tumorales se mantuvieron en forma ascítica. Los tratamientos comenzaron el tercer día después de la implantación de las células tumorales, y se realizaron evaluaciones biométricas diariamente hasta el octavo día. La microesteatosis y la necrosis coagulativa hepática, el engrosamiento de la cápsula de Bowman y la necrosis tubular renal fueron más graves con 1000 o 4000 µg/kg. **Resultados:** En general, la tasa más efectiva de inhibición tumoral se observó en animales tratados con 40 µg/kg del compuesto, con una reducción porcentual que osciló entre el 90% y el 96% en comparación con los controles. La naftoquinona no mostró un efecto anticancerígeno dependiente de la dosis. Sin embargo, se observaron alteraciones histopatológicas significativas dependientes de la dosis, particularmente en el hígado, los riñones, el corazón y el bazo, así como una disminución del hematocrito. **Conclusión:** Los datos demuestran que, si bien la naftoquinona promovió una reducción tumoral significativa a una dosis de 40 µg/kg, esto se acompañó de una marcada toxicidad dependiente de la dosis en el hígado, los riñones y el corazón.
Palabras clave: Cáncer, Carcinoma de Ehrlich, Histopatología, Química medicinal, Toxicidad.

INTRODUCTION

Cancer remains a major global health challenge, with about 19.3 million new cases and nearly 10 million deaths in 2020 (SUNG HH, et al., 2021). Metastasis is the leading cause of cancer mortality, driven by resistance to cytotoxic agents and evasion of apoptosis (FARES J, et al., 2020). Conventional chemotherapeutics often lack tumor selectivity and are associated with high toxicity, adverse effects, and drug resistance (REDIG AJ and McALLISTER SS, 2013; SAHU T, et al., 2021), highlighting the need for safer, more effective options.

Natural products, especially plant-derived compounds, have provided over 70% of approved anticancer drugs (SIDDIQUI AJ, et al., 2022). Quinones and their derivatives are particularly notable for their broad bioactivity and ability to target multiple molecular pathways (ZHANG L, et al., 2021). Several approved anticancer agents share a quinonoid structure, acting mainly through oxidative stress induction and alkylation of cellular nucleophiles (KOVACIC P and SOMANATHAN R, 2011). Lapachol and β-lapachone, two naphthoquinones from Bignoniaceae species, exhibit potent antitumor activity in vitro and in vivo but show limitations such as toxicity, poor solubility, and low bioavailability (OLIVEIRA KM, et al., 2021).

To address these issues, synthetic naphthoquinones have been developed to improve efficacy and pharmacological properties (FERRAZ DA COSTA DC, et al., 2020). For example, 2-amino-naphthoquinones synthesized by De Moraes TAP, et al. (2014) demonstrated strong cytotoxicity against leukemia and colon adenocarcinoma cell lines.

Among preclinical models, Ehrlich ascites carcinoma—a spontaneous murine mammary adenocarcinoma—has been extensively used to investigate tumor biology and screen antitumor candidates (OURIQUE F, et al., 2015).

This study evaluated the toxicity and antitumor potential of a synthetic naphthoquinone (2-N-glycine-1,4-naphthoquinone), structurally related to lapachol, in mice bearing Ehrlich tumor.

METHODS

Test drug

The drug tested is a derivative of quinone, structurally related to the basic core of lapachol (2-hydroxy-1.4-naphthoquinone), synthesized by this research group. The derivative 2-N-glycine-1.4-naphthoquinone (**Figure 1B**) was obtained by synthesis from 2-methoxy-1.4-naphthoquinone in a nucleophilic substitution reaction with glycine in methanol, in the presence of aqueous solution of 10 % potassium hydroxide (Camara CA, et al., 2008).

After neutralization, the derivative was purified using chromatographic techniques, particularly flash column of silica gel, silica gel-60 (230-400 Mesh, Fluka) using dichloromethane / methanol (Vetec) as eluent and characterized by analytical and spectroscopic methods. The melting point was obtained using a melting block heated in an appliance (Quim) and compared with published data (WIN T and BITTNER S, 2005).

Acute Toxicity

The acute toxicity of 2-N-glycine-1,4-naphthoquinone was evaluated under approval of the Animal Ethics Committee of the Federal University of Pernambuco (protocol no. 002/2023). Twenty male Swiss albino mice (8 weeks old, 45–55 g) were housed under standard conditions with ad libitum access to food and water. Animals were randomly divided into four groups (n=5) and administered a single oral dose of 120, 240, 1000, or 4000 µg/kg via gavage.

Behavioral observations were conducted continuously for 60 minutes post-dosing and at 24, 48, and 72 hours, focusing on CNS-related signs such as agitation, apathy, grooming, piloerection, tremors, exophthalmos, photophobia, tachypnea, prostration, exploratory behavior, and reflex responses.

At study end, animals were euthanized with ketamine/xylazine (240/30 mg/kg, i.m.), and liver, kidneys, heart, lungs, and spleen were collected and fixed in 10% formalin for histopathology. Dose–response effects were analyzed and graphically presented.

Antitumoral assay

After analysis of the results obtained in the acute toxicity assay, 30 mice under similar conditions previously reported were used for antitumoral evaluation of the 2-N-glycine-1.4-naphthoquinone exposure, using the Ehrlich's ascitic tumor as experimental model.

The following experimental groups, with 6 animals each, receiving the substance by gavage in a single dose: Group I – Control, receiving physiological solution; Group II – 40 µg/kg; Group III – 60 µg/Kg; Group IV – 80 µg/Kg and Group V – 100 µg/Kg.

Tumor cell lineage maintenance and tumor induction

Ehrlich's carcinoma was maintained in the peritoneal cavity of adult mice by serial intraperitoneal passages every seven days. After each passage, animals were euthanized and ascitic fluid was collected with a sterile syringe. For lineage maintenance, 10^6 viable cells were inoculated intraperitoneally into healthy recipients. T

o quantify viable cells, 1 mL of ascitic fluid was centrifuged at 2500 g for 5 min, the pellet washed three times with Ringer's solution, and resuspended in 1 mL of the same solution.

A 20 µL aliquot was diluted 1:100 in 0.025% trypan blue, and viable cells were counted in four hemocytometer quadrants. The mean value was multiplied by 16 to obtain the number of cells in 10 µL, and total viable cells per milliliter were calculated as: Cells/mL = (mean count × dilution × 10^4) / 4.

For tumor induction, 200 µL of a suspension containing 10^5–10^7 viable cells/mL was injected subcutaneously into the right axillary region of healthy mice. On day 3 post-inoculation, animals were weighed, tumor dimensions measured, and 2-N-glycine-1,4-naphthoquinone administered daily according to group until day 10, when animals were euthanized (MENDES MIRANDA SE, et al., 2021).

Induction and analysis of tumor development

Tumor volume was estimated using the formula: Volume (mm3) = (D X d2) / 2; where "D" represents the largest diameter and "d" the smallest diameter (Steel, 1987).

The % daily tumor inhibition was calculated using the formula: % Tumor Inhibition = (C - T) / C × 100; where C = average weight of tumors in control animals and T = average weight of tumors in the animals of groups treated with different concentrations of the test substance (KIM S, et al., 2001).

Histopathological and hematological measures

After euthanasia, liver, kidneys, heart, lungs, spleen, and tumors were excised, weighed, and fixed in 10% formaldehyde. Organs were processed for paraffin embedding, sectioned at 4 µm, and stained with hematoxylin-eosin.

Histopathological evaluation assessed congestion, degeneration, atrophy, necrosis, and metastasis, classified by intensity and extent (focal/mild, multifocal/moderate, diffuse/intense). Tumors were examined for necrotic areas, viable cells, vascularization, subcutaneous infiltration, and mitotic activity.

Blood was collected via cardiac puncture into anticoagulant tubes, centrifuged (2500 g, 5 min), and leukocyte counts were performed using a Neubauer hemocytometer. Differential counts were done on Panoptic-stained blood smears.

Statistical analysis

Results are presented as mean ± standard deviation. Data normality was assessed using the Shapiro–Wilk test (Statistica 7.0; StatSoft, 2022). When normality was confirmed, one-way ANOVA followed by Tukey's post hoc test was performed (GraphPad Instat®, 2022). A 5% significance level was adopted for all analyses.

RESULTS

Acute Toxicity

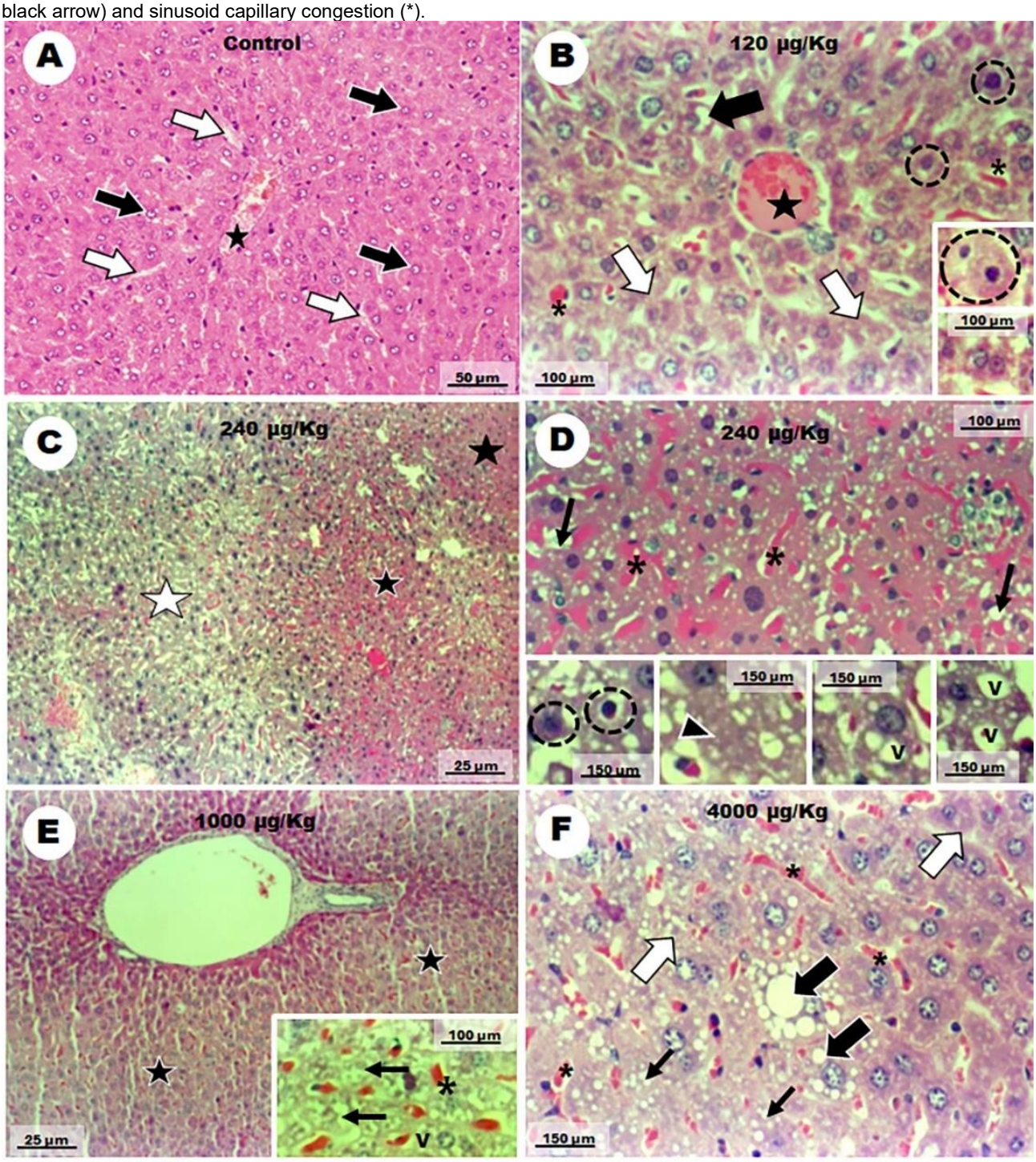
Histopathological Analysis

The acute toxicity assessment of 2-N-glycine-1,4-naphthoquinone revealed no mortality at doses up to 4000 µg/kg within a 72-hour observation period, preventing determination of a definitive LD_{50}. Despite the absence of lethality, histopathological analysis revealed dose-dependent tissue damage in multiple organs, as illustrated in **Figures 1–4**.

In the liver, animals treated with 120 µg/kg exhibited mild sinusoidal, central-lobular, and portal vein congestion. Discrete diffuse central-lobular microsteatosis and multifocal coagulative necrosis were observed, along with reactive hepatocytes showing enlarged cytoplasm and nuclei, prominent nucleoli, and loose chromatin.

Mitotic figures were noted near portal areas. At 240 µg/kg, liver lesions intensified, including severe sinusoidal and central-lobular congestion, extensive coagulative necrosis near the portal triad, and marked macro- and microsteatosis, accompanied by nuclear abnormalities.

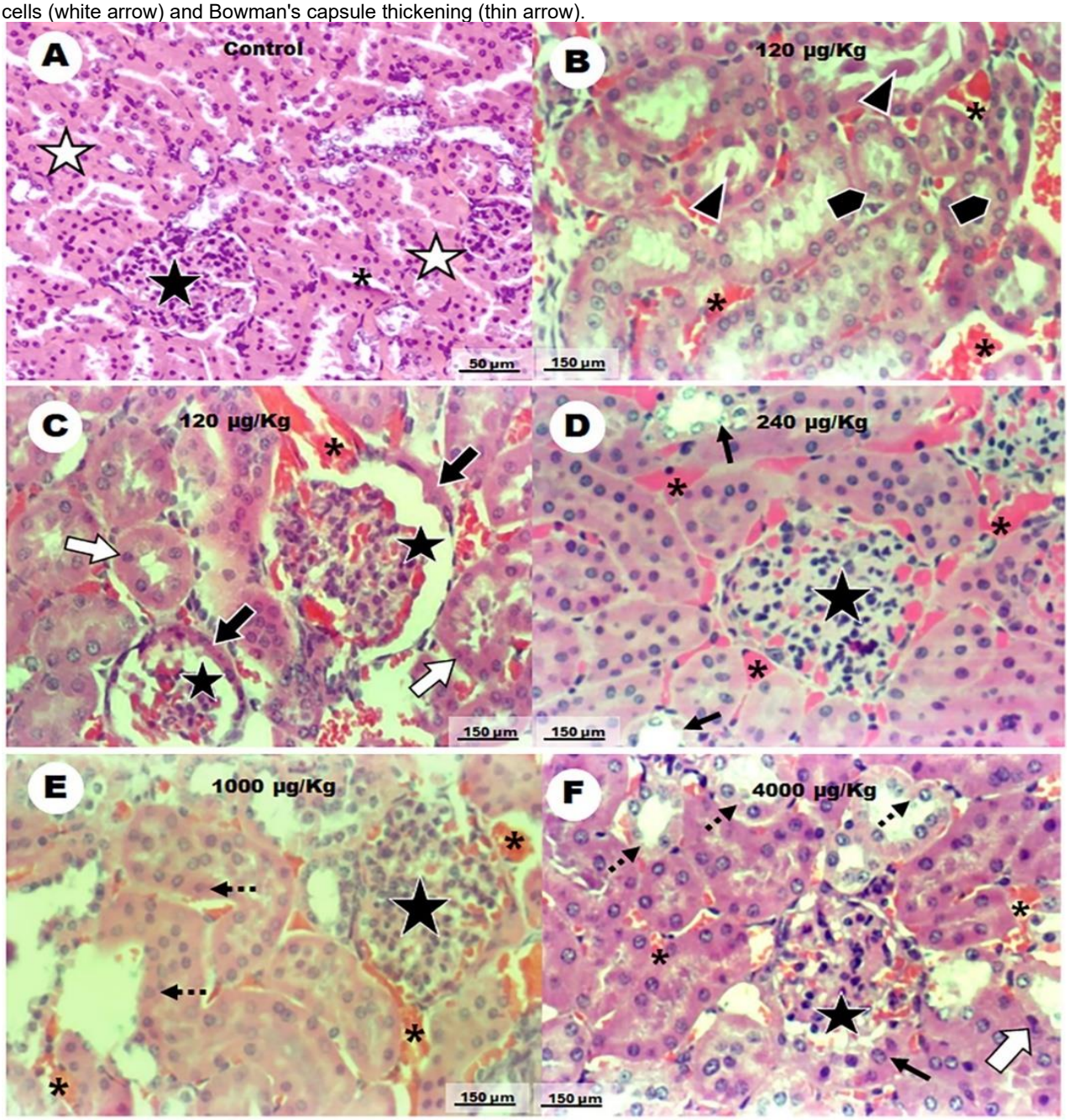
Figure 1 - Histopathological analysis of the liver of mice with Ehrlich's ascitic tumor and treated with physiological solution (A), 120 µg/Kg (B), 240 µg/Kg (C-D), 1000 µg/Kg (E) or 4000 µg/Kg (F) of 2-N-glycine-1,4-naphthoquinone. A: Liver parenchyma with normal appearance in hepatocytes (black arrow), sinusoid capillaries (white arrow), and central-lobular vein (black star). B: Liver parenchyma with slight congestion of sinusoid capillaries (*), congestion of the central-lobular vein (black star); coagulation necrosis of periportal hepatocytes (white arrow), cytoplasmic vacuolation (black arrow), different degrees of nuclear pyknosis (dashed line and upper detail) and binucleated hepatocytes (lower detail). C: Liver parenchyma of mice with intense diffuse congestion (black star) and periportal coagulation necrosis (white star). D: Detail of the hepatic parenchyma with intense congestion of sinusoid capillaries (*) and macrosteatosis (thin arrow). In the details, note the necrotic area with cells with pyknotic nucleus (dashed), cell without nucleus (arrowhead) and cytoplasmic vacuoles (V). E: Liver parenchyma with congestion in periportal sinusoid capillaries and periportal coagulation necrosis (black star). In the detail, congestion in sinusoidal capillaries (*), necrosis (thin arrow) and cytoplasmic vacuolation (V) can be seen. F: Liver parenchyma with different degrees of necrosis (white arrow), macrosteatosis (large black arrow), microsteatosis (thin black arrow) and sinusoid capillary congestion (*).



Source: Silva ECS, et al., 2026.

Renal tissue showed proliferative glomerulitis, glomerular atrophy, and corticomedullary congestion at 120 µg/kg, along with hydropic degeneration, nephrosis, and tubular protein casts. At 240 µg/kg, lesions progressed to glomerular sclerosis, thickening of Bowman's capsule, and extensive necrosis of proximal and distal tubules, indicating increasing nephrotoxicity.

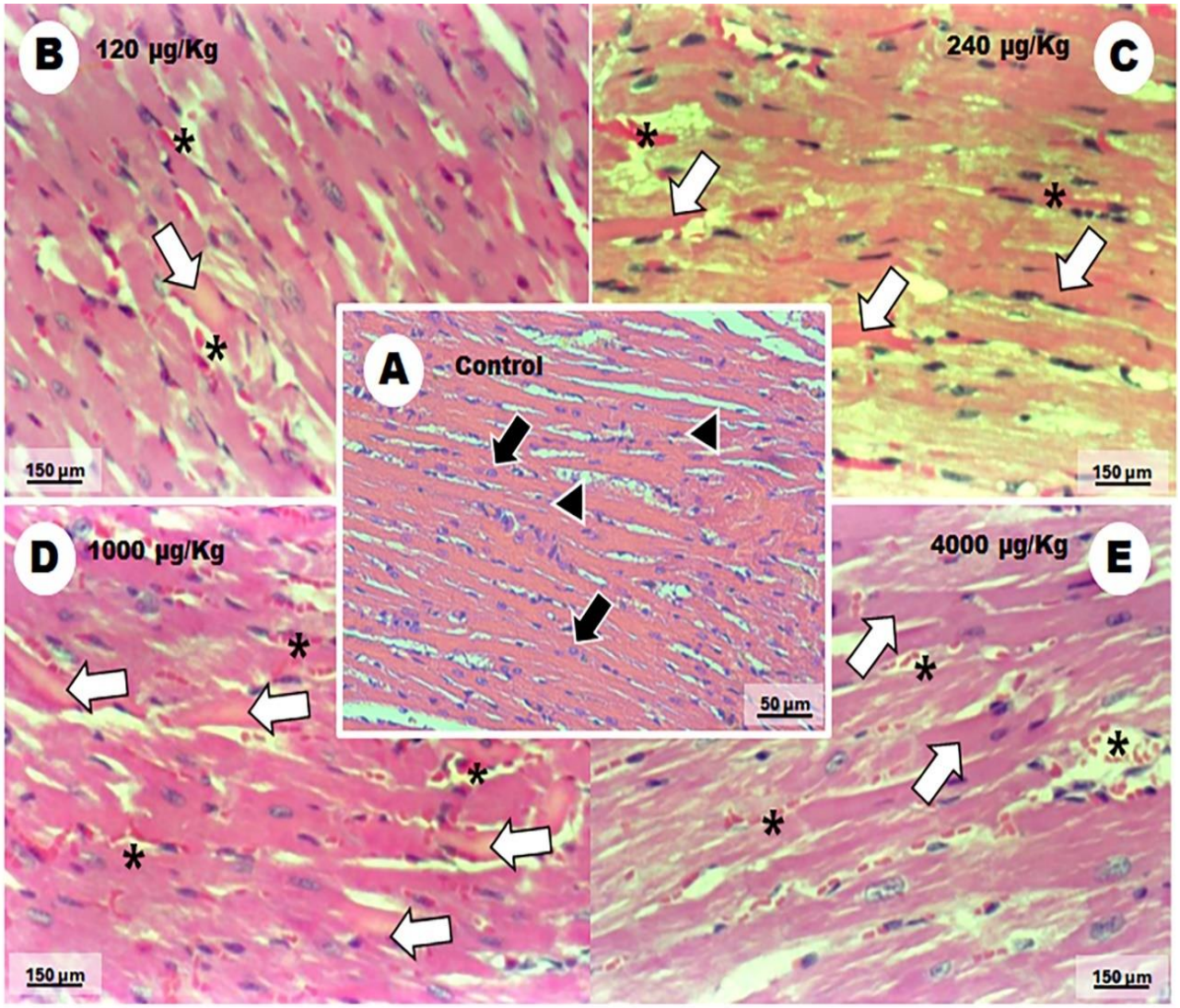
Figure 2 - Histopathological analysis of the kidney of mice with Ehrlich's ascitic tumor and treated with physiological solution (**A**), 120 µg/Kg (**B-C**), 240 µg/Kg (**D**), 1000 µg/Kg (**E**) or 4000 µg/Kg (**F**) of 2-N-glycine-1,4-naphthoquinone. **A:** Renal parenchyma with normal appearance of convoluted tubules (white star), glomeruli (black star) and capillaries (*). **B:** Renal parenchyma with protein casts in the lumen of the convoluted tubules (arrowhead), intense vascular congestion (*), and turbid swelling with increased cell volume (pentagon). **C:** Glomerular atrophy (black star) with thickening of Bowman's capsule (black arrow) and tubular cell pyknosis (white star). **D:** Proliferative glomerulonephritis (black star), necrosis of cells in the wall of the convoluted tubules (thin black arrow) and severe renal congestion (*). **E:** Renal parenchyma with congestion (*), hydropic degeneration (dashed arrow) and proliferative glomerulonephritis (star). **F:** Renal parenchyma with hydropic degeneration of the renal tubules (dashed arrow), renal congestion (*), glomerular atrophy (star), necrotic cells (white arrow) and Bowman's capsule thickening (thin arrow).



Source: Silva ECS, et al., 2026.

Cardiac tissue exhibited intense vascular congestion, hydropic degeneration, and loss of transverse striations in cardiomyocytes. Eosinophilia and discrete coagulative necrosis were present, becoming more prominent with dose escalation. Myocardial vacuolization and structural disorganization were notable at higher doses.

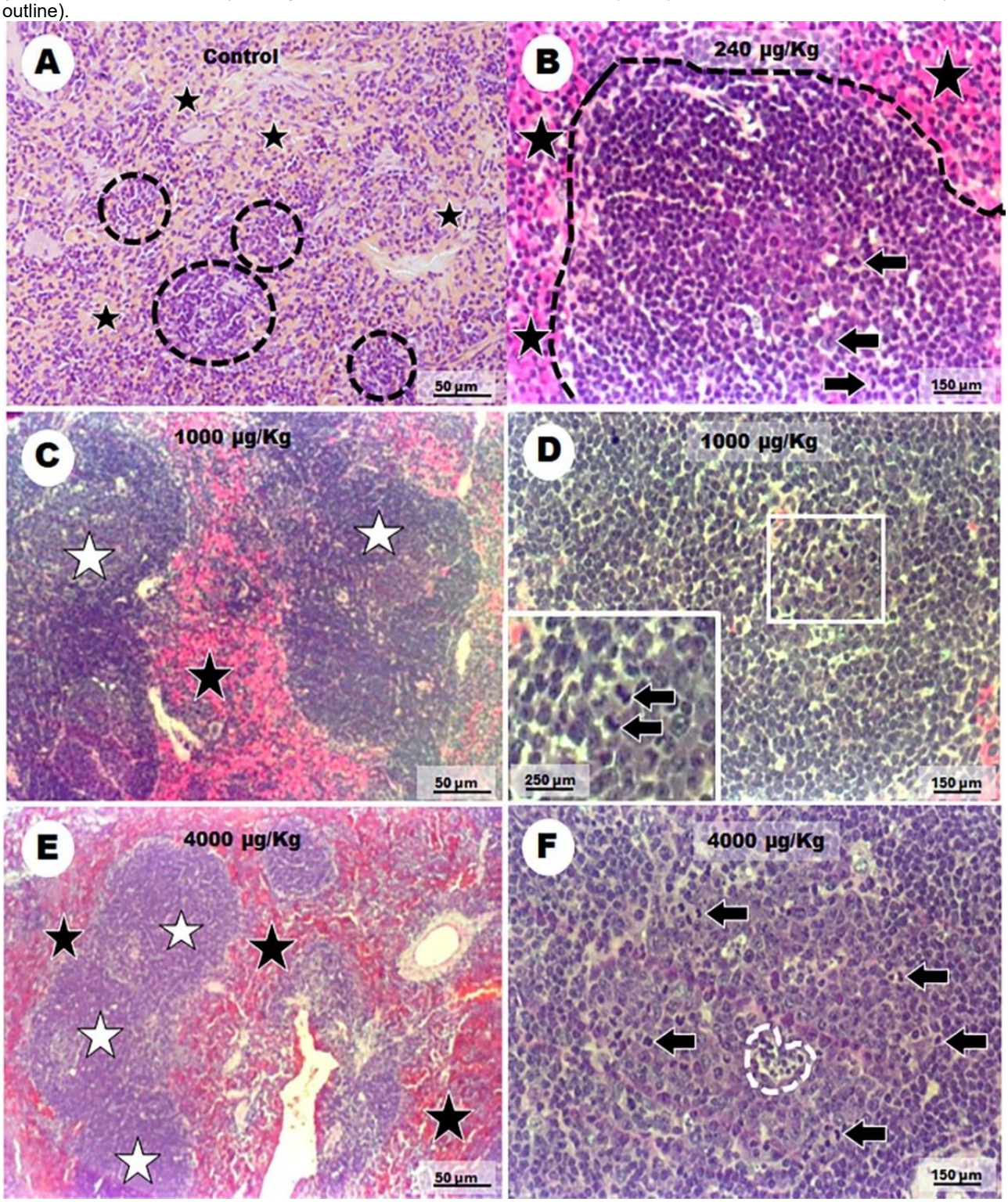
Figure 3 - Histopathological analysis of the heart of mice with Ehrlich's ascitic tumor and treated with physiological solution (A), 120 µg/Kg (B), 240 µg/Kg (C), 1000 µg/Kg (D) or 4000 µg/Kg (E) of 2-N-glycine-1,4-naphthoquinone. Figure A shows the normal histology of the heart, with myocardial cells in longitudinal sections (black arrow) and capillaries among these cells (arrowhead). On the figures B to E it is shown myocardium in longitudinal section, where cardiomyocytes had lost of transverse striation, coagulation necrosis (white arrow), mild to moderate congestion (*) and cellular eosinophilia; the last one similar to the observed in the control group.



Source: Silva ECS, et al., 2026.

The spleen displayed relatively preserved architecture across groups but consistently showed red pulp congestion. Additional findings included megakaryocyte vacuolization and necrosis, mild hemosiderin accumulation in macrophages, and white pulp hyperplasia with mitotic lymphocytes, lymphoid nodule fusion, and focal lymphocyte necrosis and apoptosis.

Figure 4 - Histopathological analysis of the spleen of mice with Ehrlich's ascitic tumor and treated with physiological solution (**A**), 240 µg/Kg (**B**), 1000 µg/Kg (**C-D**) or 4000 µg/Kg (**E-F**) of 2-N-glycine-1,4-naphthoquinone. **A:** Normal histology of spleen parenchyma, showing the white (dashed lines) and red (star) pulps. **B:** Splenic lymphoid nodule (dashed outline) showing hyperplasia of the germinal center, where mitotic figures can be seen (arrow). It is also noted a red pulp congestion (black star). **C:** Splenic parenchyma with red pulp congestion (black star) and white pulp hyperplasia (white star). **D:** Splenic lymphoid nodule with the presence of mitotic figures (thin arrow). **E:** Splenic parenchyma with white pulp hyperplasia (white star) and fusion of lymphoid nodules (white star), and intense organ congestion (black star). **F:** Intense activation of germinal centre, showed by the figures of mitotic division on white pulp (arrow) and clusters of apoptotic cells (dashed outline).



Source: Silva ECS, et al., 2026.

At 1000 and 4000 µg/kg, lesions were more severe and widespread. The liver presented diffuse steatosis and extensive hepatocyte necrosis. Kidneys exhibited exacerbated glomerular damage and massive tubular necrosis. Myocardial lesions were intensified, with pronounced vacuolization and degeneration. The spleen showed persistent white pulp hyperplasia and germinal center activation.

Behavior analysis

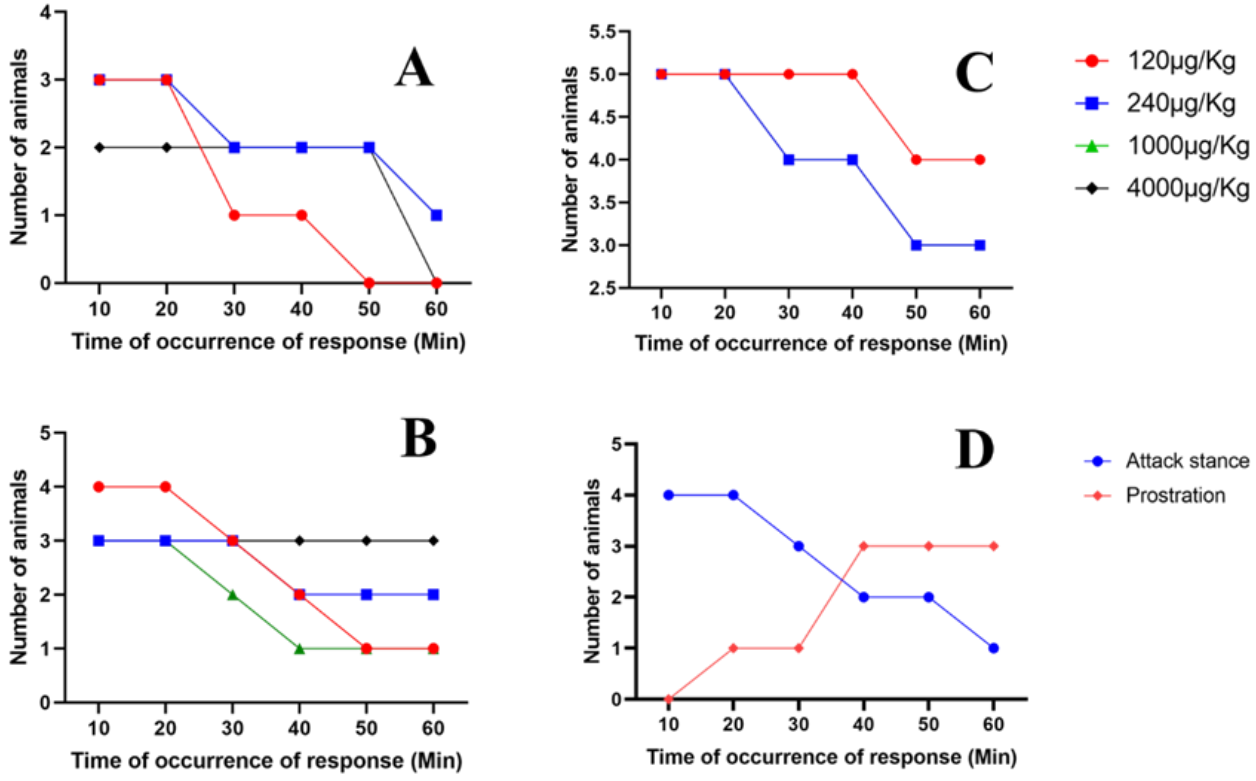
The study observed several responses suggestive of central nervous system (CNS) stimulation, with specific timing and intensity during the first 60 minutes (**Figure 5**). After the lower drug dose, animals showed behaviors indicative of CNS stimulation, including exploratory behavior, agitation, circular movements, vibrissae movement, claw posture, and attack posture. These behaviors followed a similar decreasing pattern over time. A comparable trend occurred at 1000 µg/kg for vibrissae movement, agitation, and circular movements.

Circular movements (**Figure 5A**), agitation (**Figure 5B**), and vibrissae movement (**Figure 5C**) at 120 µg/kg were most pronounced in the first 20 minutes post-administration, significantly decreasing over the 60-minute observation period. Exploratory behavior peaked around 30 minutes before declining. Vibrissae movement persisted in all animals for 40 minutes before tapering off.

Attack posture (**Figure 5D**) and claw posture peaked within the initial 20 minutes, gradually diminishing over the remaining observation period. Additionally, petechiae on the tail and muzzle edema were present for 60 minutes.

In contrast, depressive effects on the CNS were observed. Prostration (**Figure 5D**) and grouping behaviors increased as exploratory behavior declined, becoming more pronounced in the final observation stage.

Figure 5 - Behavioral changes and response time in mice with Ehrlich ascites tumor and treated with different concentrations of 2-N-glycine-1,4-naphthoquinone, under analysis of spontaneous behavior. **A-** Circular movement; **B-** Agitation; **C-** Vibrating movement; **D-** attack posture and reactions of prostration present only in the dose 120µg/Kg. **120µg/Kg** - red line with ball; **240µg/Kg** - Blue line with square; **1000µg/Kg** - Green line with triangle; **4000µg/Kg** - black line with diamond.



Source: Silva ECS, et al., 2026.

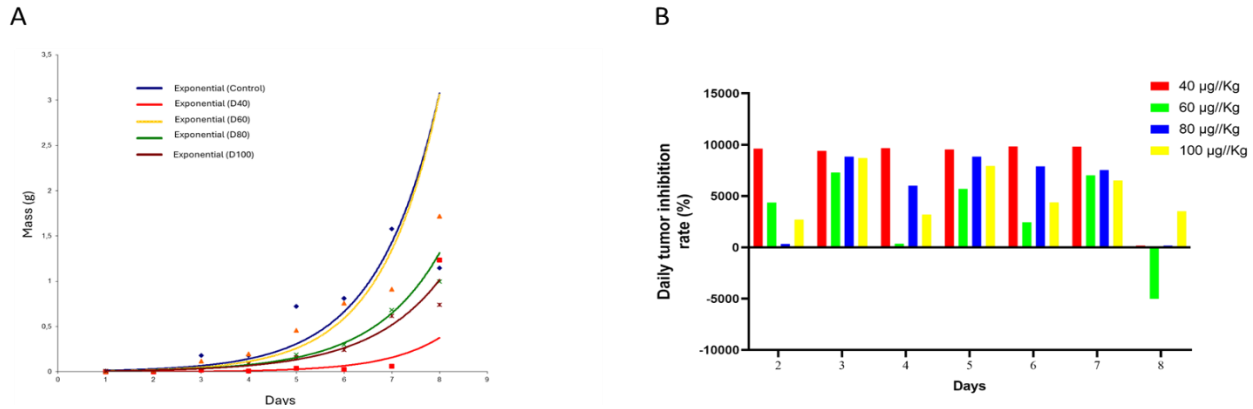
Antitumor Assay

Tumor development and macroscopic analyses

The body weight of mice treated with 2-N-glycine-1,4-naphthoquinone remained consistent across all groups, showing no significant differences from the control group. **Figure 6** presents the evaluation of mean tumor mass evolution. On the first day of measurement, there were no significant differences between groups. However, by the second day, a substantial reduction in tumor mass was observed in animals treated with 40 µg/kg of the compound compared to both the control and the 80 µg/kg group. This decreasing trend in tumor mass continued on the third day and was even more pronounced by the fourth and fifth days, with the 40 µg/kg group consistently showing the greatest reduction in tumor volume compared to the control and other treatment groups. On the sixth and seventh days, tumor mass remained significantly lower in the 40 µg/kg group, showing marked suppression compared to the control and the 60 µg/kg group. By the final day of treatment, no significant differences were observed between the treatment groups regarding tumor mass.

Figure 6A illustrates tumor mass progression over time. Tumor growth followed an exponential pattern for each dose group. Among them, the 40 µg/kg dose showed the most effective reduction in tumor mass throughout the observation period. Figure 6B shows the estimated daily tumor inhibition percentage. The 40 µg/kg dose demonstrated the highest average inhibition rate across all days, followed by the 80 and 100 µg/kg groups. In contrast, the 60 µg/kg group showed the lowest tumor inhibition and the highest tumor weight among the treated groups.

Figure 6 - Antitumor effects of 2-N-glycine-1,4-naphthoquinone in Swiss mice bearing Ehrlich tumor.



(A) Evolution of tumor weight (mg) in Swiss mice treated with different doses of 2-N-glycine-1,4-naphthoquinone during the experimental period. (B) Daily tumor inhibition rate (%) in treated mice compared with the control group over the 8-day experimental period. Data are expressed as mean ± standard deviation. **Source:** Silva ECS, et al., 2026.

Regarding organ weight, a significant reduction in spleen weight was found in mice treated with 100 µg/kg compared to those receiving 60 µg/kg (**Table S1**). This reduction may be associated with white pulp hypoplasia and increased apoptosis of lymphocytes in germinal centers. Mice treated with 80 µg/kg exhibited a similar trend in spleen weight reduction and histopathological findings, closely resembling those observed in the 100 µg/kg group.

Histopathological and hematological analysis

Histopathological examination revealed liver microsteatosis and sinusoidal congestion in all groups, including controls. Coagulative necrosis varied with dose: mild and pericentral at the lowest dose, moderate and diffuse at 60 µg/kg, and more severe at 80 and 100 µg/kg. Mild periportal hepatitis appeared at 40 µg/kg, while 60 µg/kg caused marked Kupffer cell activation, scattered lymphocytes, and mild focal periportal hepatitis. At 80 µg/kg, steatonecrosis was evident, and 100 µg/kg produced intense, diffuse lymphomononuclear infiltrates around metastatic foci, including subcapsular regions (**Figure S1 A**).

In the kidneys, 40 µg/kg induced proliferative glomerulonephritis, Bowman's capsule thickening, and focal tubular necrosis. Lesions worsened at 80 and 100 µg/kg, showing corticomedullary congestion, glomerular atrophy, protein casts, and marked hydropic degeneration with tubular necrosis at 100 µg/kg (**Figure S1 B**). Hearts of controls showed mild cardiomyocyte congestion and necrosis, whereas treated animals exhibited more severe myocardial congestion, lymphomononuclear infiltrates, cardiomyocyte vacuolation, loss of transverse striation, and multifocal coagulative necrosis, indicating dose-dependent cardiotoxicity (**Figure S1 C**). Lungs displayed mild–moderate congestion, type II pneumocyte activation, chronic interstitial pneumonia, alveolar wall thickening, and emphysema across all groups, changes likely unrelated to treatment. Metastatic foci appeared in animals receiving 40 or 100 µg/kg (**Figure S1 D**). At 80 and 100 µg/kg, spleens showed red pulp congestion, white pulp hypoplasia, and apoptotic lymphocyte foci in germinal centers and the marginal zone.

Tumors from all groups exhibited central necrosis, viable cells among necrotic areas, and vascular proliferation (**Figure S1 E–F**). Controls additionally presented dystrophic calcification, abundant polymorphonuclear cells, and viable cells near subcutaneous muscle. At 40 µg/kg, tumors displayed large peripheral necrosis with multiple viable-cell foci. In the 60 and 80 µg/kg groups, tumors showed central necrosis, peripheral viable cells, apoptotic figures, low mitotic activity, and scattered polymorphonuclear cells.

Hematological evaluation revealed a significant reduction in hematocrit levels in animals treated with 60 µg/kg compared to the control. However, leukocyte counts—including total leukocytes, bands, segmented neutrophils, lymphocytes, and monocytes—did not show significant differences between groups (**Table S2**).

DISCUSSION

Acute toxicity

The behaviors suggestive of central nervous system (CNS) stimulation observed in healthy animals exposed to various doses of the tested compound are likely associated with excitatory mechanisms induced by the drug. The intensity of these responses may be linked to processes of excretion or biotransformation (ABERNETHY DR, et al., 1986).

Some effects appear to involve activation of the sympathetic component of the autonomic nervous system (ANS), such as the agitation and increased exploratory behavior recorded (MATTEI R, et al., 2006). Stereotyped movements, mood disturbances, vibrissae twitching, and circling behaviors may reflect dopaminergic and noradrenergic modulation in specific CNS regions (MATTEI R, et al., 2006; OVERALL KL, 1994).

The presence of petechiae on the tail and sustained muzzle edema—both persisting for approximately 60 minutes—indicate significant vascular alterations, potentially related to sympathetic stimulation. The ANS plays a key role in regulating vascular parameters, including vessel tone, pulse wave dynamics, cardiac output, and blood volume (MANCIA G and GRASSI G, 2014; ZHANG DY and ANDERSON AS, 2014).

These vascular manifestations may also involve other endogenous mediators, such as pro-inflammatory pathways and immune system activation, which could contribute to tissue-specific effects or hypersensitivity reactions (KRÜGER-GENGE A, et al., 2019; ZHANG HS, et al., 2019).

Histopathological findings suggest that hypertension may have contributed to the petechial hemorrhages observed in the tail, nasal swelling, and the intense pulmonary congestion reported in this study. Conversely, immediate hypersensitivity reactions were considered unlikely due to the absence of mucus in airway tissue samples (bronchi and bronchioles), along with the lack of perivascular or interstitial pulmonary edema and eosinophilic infiltration.

The dose-dependent increase in behaviors associated with CNS excitation—such as circling, agitation, vibrissae movements, and exploratory activity-supports the hypothesis of a pharmacological effect proportional to the administered dose. Specifically, circling behavior and agitation may serve as indicative behavioral models reflecting both the intensity of the response and the drug dosage.

Antitumoral assay

Tumor development and macroscopic analysis

The antitumoral treatment with 2-N-glycine-1.4-naphthoquinone did not markedly affect changes in body weight of the animals, similar to findings previously observed with administration of lapachol, a structurally related quinone (GUERRA MO, et al., 2001).

On the other hand, when measuring the tumoral mass during the experimental period, the 40 µg/kg dose of the drug tested exhibited significant antitumoral activity, similar or greater than that observed for lapachol both in vivo and in vitro (MENDES MIRANDA SE, et al., 2021), as well for other quinones (TSAO YC, et al., 2020)

The spleen was the only organ that showed mass variation, which decreased when mice received 100 µg/kg naphthoquinone. This finding may reflect an impairment in the hematopoietic and immune system, since the spleen is a crucial site of innate and adaptive immune regulation, and tumor-derived secretory factors may affect splenic hematopoietic and stromal cells to initiate metastasis (STEENBRUGGE J, et al., 2021).

Histopathological and hematological analyses

Microsteatosis, diffusely observed across all treatment groups, indicates severe liver dysfunction or toxicity commonly associated with neoplastic conditions (ANGULO P, 2002; NARAYAN RR, et al., 2020). This lesion is linked to mitochondrial β-oxidation impairment and often arises from exposure to drugs, toxins, or metabolic disorders (JOLLY RA, et al., 2004). Additionally, it may reflect disruptions in hepatic cellular transport and VLDL secretion (FROMENTY B, et al., 1997). Such hepatotoxicity challenges drug development due to delayed histological manifestation in animal models (JOLLY RA, et al., 2004).

Coagulative necrosis was prominent, particularly at 80 and 100 µg/kg doses. Drug-induced hepatic ischemia, resulting from altered oxygen gradients in the liver's biotransformation zones, leads to reactive metabolite formation, oxidative stress, and lipid peroxidation of membranes. The centrilobular necrosis observed likely reflects vascular congestion and impaired perfusion (MOTA BANDARRA P, et al., 2009).

The kidney, vulnerable to drug-induced injury (SINGH AK, et al., 2022), showed nephrotoxicity at 80 and 100 µg/kg, suggesting impaired renal perfusion. This is typical with renally excreted drugs, especially in overdose, causing elevated intratubular concentrations, crystal precipitation, and urinary obstruction (PERAZELLA MA, 2018). Histology revealed acute tubular necrosis, glomerular injury, and tubular dysfunction.

Cardiac tissue exhibited marked cardiomyocyte toxicity at higher doses, surpassing lesions in untreated tumor-bearing controls. Cardiotoxicity is a known limitation of many anticancer agents (PONNAPAKKAM T, et al., 2021), consistent with reports on other naphthoquinones (GORNOSTAEV LM, et al., 2017). These data emphasize the need to define therapeutic windows balancing efficacy and cardiac safety, given the risk of irreversible cardiovascular damage (CURIGLIANO G, et al., 2012).

Pulmonary alterations were milder but included subtle interstitial changes and pneumocyte involvement. Considering the lungs' sensitivity to anticancer drugs and quinone toxicity, these findings are relevant (KUPFER R, et al., 2002). Pulmonary inflammation and interstitial lung disease are recognized chemotherapy side effects (FERNANDO IN, et al., 1996). Spleen histology at 80 and 100 µg/kg revealed red and white pulp alterations, including lymphocyte apoptosis in germinal centers and marginal zones, with reduced spleen weight, indicating potential immunosuppression and hematopoietic impairment (STEENBRUGGE J, et al., 2021).

Tumor necrosis was mainly coagulative, with polymorphonuclear infiltration typical of necrotic inflammation (RAMALHO RT, et al., 2014). Apoptotic nuclear and cytoplasmic degradation was evident in all groups, most notably at 40 µg/kg, correlating with tumor mass reduction and suggesting a therapeutic effect. Hematocrit was significantly reduced at 60 µg/kg, indicating systemic compromise. In cancer patients, anemia correlates with increased morbidity and mortality, underscoring the clinical importance of this finding (CHEN M, et al., 2020).

This study presents promising antitumor and toxicological findings; however, some limitations should be acknowledged. The sample size and observation period, although adequate for an initial evaluation, may limit broader extrapolations. In addition, the absence of a reference drug restricts direct comparisons with established therapies, and mechanistic aspects were not explored in depth. Future studies should expand these findings by including longer experimental periods, comparative analyses with standard chemotherapeutics, and investigations into the molecular mechanisms involved, particularly those related to oxidative stress and apoptosis.

CONCLUSION

The acute toxicity test revealed a stimulating effect of 2-N-glycine-1.4-naphthoquinone on the central nervous system, suggesting a dose-dependent pharmacological effect, and the histopathological analysis of acute toxicity findings of liver, kidneys, heart and spleen revealed greater intensity of lesions at 1000 and 4000 µg/kg naphthoquinone. In the antitumoral assay, although naphthoquinone promoted a significant tumor reduction at a dose of 40 µg/kg greater than 90%, dose-dependent toxicity was observed in organs examined. The antitumoral results enables us to suggest that further investigations need to be conducted by administering 2-N-glycine-1.4-naphthoquinone in different lower dosages.

ACKNOWLEDGEMENTS

This study was funded by PhD scholarship provided to FCRD, Fundação de Amparo à Pesquisa do Estado de Minas Gerais, for financial support (grant number BPD 00733-22).

REFERENCES

1. ABERNETHY DR, et al. Benzodiazepine hypnotic metabolism: drug interactions and clinical implications. Acta Psychiatr Scand Suppl, 1986; 332: 32–38.
2. DE OLIVEIRA VA, et al. α-tocopherol as a selective modulator of toxicogenic damage induced by antineoplastic agents cyclophosphamide and doxorubicin. Journal of Toxicology and Environmental Health Part A, 2023; 86: 87–102.
3. EPIFANO F, et al. Lapachol and its congeners as anticancer agents: A review. Phytochemistry Reviews, 2014.
4. FARES J, et al. Molecular principles of metastasis: a hallmark of cancer revisited. Signal Transduction and Targeted Therapy, 2020.
5. FERRAZ DA COSTA DC, et al. Anticancer potential of resveratrol, β-lapachone and their analogues. Molecules, 2020; 25.
6. KIM S, et al. Cytotoxic alkaloids from Houttuynia cordata. Archives of Pharmacal Research, 2001; 24: 518–521.
7. KOVACIC P e SOMANATHAN R. Anti-cancer agents in medicinal chemistry. Anti-Cancer Agents in Medicinal Chemistry, 2011.
8. KRÜGER-GENGE A, et al. Vascular endothelial cell biology: An update. International Journal of Molecular Sciences, 2019; 20.
9. MANCIA G e GRASSI G. The autonomic nervous system and hypertension. Circulation Research, 2014.
10. MATTEI R, et al. Psicofarmacologia: fundamentos práticos. 1 ed. Rio de Janeiro: Guanabara Koogan, 2006.
11. MENDES MIRANDA SE, et al. Enhanced antitumor efficacy of lapachol-loaded nanoemulsion in breast cancer tumor model. Biomedicine and Pharmacotherapy, 2021; 133.
12. OLIVEIRA KM, et al. Lapachol in the design of a new Ruthenium(II)-Diphosphine complex as a promising anticancer metallodrug. Journal of Inorganic Biochemistry, 2021; 214.
13. OURIQUE F, et al. DNA damage and inhibition of akt pathway in MCF-7 cells and ehrlich tumor in mice treated with 1,4-naphthoquinones in combination with ascorbate. Oxidative Medicine and Cellular Longevity, 2015; 2015.
14. OVERALL KL. Use of clomipramine to treat ritualistic stereotypic motor behavior in three dogs. Journal of the American Veterinary Medical Association, 1994; 205: 1733–1741.

15. REDIG AJ e MCALLISTER SS. Breast cancer as a systemic disease: A view of metastasis. Journal of Internal Medicine, 2013.
16. SAHU T, et al. Nanotechnology based drug delivery system: Current strategies and emerging therapeutic potential for medical science. Journal of Drug Delivery Science and Technology, 2021.
17. SIDDIQUI AJ, et al. Plants in anticancer drug discovery: From molecular mechanism to chemoprevention. BioMed Research International, 2022.
18. SUNASSEE SN, et al. Cytotoxicity of lapachol, β-lapachone and related synthetic 1,4-naphthoquinones against oesophageal cancer cells. European Journal of Medicinal Chemistry, 2013; 62: 98–110.
19. SUNG H, et al. Global cancer statistics 2020: GLOBOCAN estimates of incidence and mortality worldwide for 36 cancers in 185 countries. CA: A Cancer Journal for Clinicians, 2021; 71: 209–249.
20. WORLD CANCER RESEARCH FUND. Worldwide cancer data. 2022. Disponível em: https://www.wcrf.org/cancer-trends/worldwide-cancer-data/ Acessado em: 12 de março de 2022.
21. ZHANG DY e ANDERSON AS. The sympathetic nervous system and heart failure. Cardiology Clinics, 2014.
22. ZHANG HS, et al. Atorvastatin suppresses vascular hypersensitivity and remodeling induced by transient adventitial administration of lipopolysaccharide in rats. Annals of Translational Medicine, 2019; 7: 386.
23. ZHANG L, et al. Recent advances of quinones as a privileged structure in drug discovery. European Journal of Medicinal Chemistry, 2021.
24. DE MORAES TAP, et al. Synthesis and cytotoxic evaluation of a series of 2-amino-naphthoquinones against human cancer cells. Molecules, 2014; 19(9): 13188–13199.
25. CURIGLIANO G, et al. Cardiovascular toxicity induced by chemotherapy, targeted agents and radiotherapy: ESMO clinical practice guidelines. Annals of Oncology, 2012; 23.
26. ANGULO P. Nonalcoholic fatty liver disease. New England Journal of Medicine, 2002; 346: 1221–1231.
27. KUPFER R, et al. Lung toxicity and tumor promotion by hydroxylated derivatives of 2,6-di-tert-butyl-4-methylphenol (BHT) and 2-tert-butyl-4-methyl-6-iso-propylphenol: Correlation with quinone methide reactivity. Chemical Research in Toxicology, 2002; 15: 1106–1112.
28. FERNANDO IN, et al. An acute toxicity study on the effects of synchronous chemotherapy and radiotherapy in early stage breast cancer after conservative surgery. Clinical Oncology, 1996.
29. STEENBRUGGE J, et al. Splenic hematopoietic and stromal cells in cancer progression. Cancer Research, 2021; 81: 27–35.
30. RAMALHO RT, et al. Histopathological evaluation of tumor necrosis and volume after cyanogenic chemotherapy. Acta Cirúrgica Brasileira, 2014; 29: 38–42.
31. PONNAPAKKAM T, et al. Acute toxicity evaluation of a novel ceramide analog for the treatment of breast cancer. Toxicology Reports, 2021; 8: 1521–1526.
32. PERAZELLA MA. Pharmacology behind common drug nephrotoxicities. Clinical Journal of the American Society of Nephrology, 2018; 13: 1897–1908.
33. SINGH AK, et al. Efficacy and safety of daprodustat for treatment of anemia of chronic kidney disease in incident dialysis patients: a randomized clinical trial. JAMA Internal Medicine, 2022; 182: 592–602.
34. MOTA BANDARRA P, et al. Avaliação histopatológica em estudo experimental. Ciência Rural, 2009; 39(1): 262–265.
35. JOLLY RA, et al. Microvesicular steatosis induced by a short chain fatty acid: effects on mitochondrial function and correlation with gene expression. Toxicologic Pathology, 2004; 32: 19–25.
36. FROMENTY B, et al. Microvesicular steatosis and steatohepatitis: role of mitochondrial dysfunction and lipid peroxidation. Journal of Hepatology, 1997; 26: 13–22.
37. NARAYAN RR, et al. Prediction of recurrence patterns from hepatic parenchymal disease after resection of colorectal liver metastases. Annals of Surgical Oncology, 2020; 27: 188–195.
38. TSAO YC, et al. Discovery of isoplumbagin as a novel NQO1 substrate and anti-cancer quinone. International Journal of Molecular Sciences, 2020; 21: 1–17.
39. GUERRA M, et al. Toxicology of lapachol in rats: embryolethality. Revista Brasileira de Biologia.
40. GORNOSTAEV LM, et al. The oxime derivatives of 1-R-1H-naphtho[2,3-d][1,2,3]triazole-4,9-dione 2-oxides: synthesis and properties. Anti-Cancer Agents in Medicinal Chemistry, 2017; 17: 1814–1823.
41. CAMARA CA, et al. Molluscicidal activity of 2-hydroxy-[1,4]naphthoquinone and derivatives. Revista Brasileira de Farmacognosia, 2008; 18: 329–334.
42. MORAES TAP, et al. Role of synthetical amynoquinone ethyl 2-(1,4-dioxo-1,4-dihydronaphthalen-2-ylamino) acetate in inhibition of Ehrlich's tumor. Pathology Research and Practice, 2023; 241.
43. CHEN M, et al. The plant natural product 2-methoxy-1,4-naphthoquinone stimulates therapeutic neural repair properties of olfactory ensheathing cells. Scientific Reports, 2020; 10.
44. WIN T e BITTNER S. Novel 2-amino-3-(2,4-dinitrophenylamino) derivatives of 1,4-naphthoquinone. Tetrahedron Letters, 2005; 46: 3229–3231.